THE ASTROPHYSICAL JOURNAL, 525:517–523, 1999 November 1

LARGE-SCALE FLOWS IN THE SOLAR INTERIOR: EFFECT OF ASYMMETRY IN PEAK PROFILES

SARBANI BASU
Institute for Advanced Study, Olden Lane, Princeton, NJ 08540

AND

H. M. ANTIA
Tata Institute of Fundamental Research, Homi Bhabha Road, Mumbai 400005, India

Received 1999 April 6; accepted 1999 June 23

ABSTRACT

Ring diagram analysis can be used to study large-scale velocity fields in the outer part of the solar convection zone. All previous works assume that the peak profiles in the solar oscillation power spectrum are symmetrical. However, it has now been demonstrated that the peaks are not symmetrical. In this work we study how the explicit use of asymmetrical peak profiles in ring diagram analysis influences the estimated velocity fields. We find that the use of asymmetrical profiles leads to significant improvement in the fits, but the estimated velocity fields are not substantially different from those obtained using a symmetrical profile to fit the peaks. The resulting velocity fields are compared with those obtained by other investigators.

Subject headings: Sun: interior — Sun: oscillations — Sun: rotation

1. INTRODUCTION

Ring diagram analysis has been used extensively to infer horizontal flows in the outer part of the solar convection zone (Hill 1988; Patrón et al. 1997; Basu, Antia, & Tripathy 1999). This technique is based on the study of three-dimensional power spectra of solar *p*-modes on a part of the solar surface. In all the studies so far, the power spectra have been fitted to symmetrical Lorentzian peak profiles in order to calculate the frequency shifts due to velocity field. It has been demonstrated that, in general, the peaks in solar oscillation power spectra are not symmetrical (Duvall et al. 1993; Toutain 1993; Nigam & Kosovichev 1998; Toutain et al. 1998) and the use of symmetrical profiles may cause the fitted frequency to be shifted away from the true value. The resulting frequency shift in the high-degree modes using ring diagram analysis has been found to be significant for *f*-modes and low-order *p*-modes (Antia & Basu 1999). Thus, it would be interesting to study how the use of asymmetrical profiles affects the measurement of flow velocities.

In this work we use the data obtained by the Michelson Doppler Imager (MDI) on board the *Solar and Heliospheric Observatory* (*SOHO*) to measure the flow velocities in the outer part of the solar convection zone. We fit the power spectra using asymmetrical peak profiles and compare the results with our earlier results obtained using symmetrical profiles (Basu et al. 1999). Although it is possible to study the variation in horizontal velocity with both longitude and latitude, in this work, as in Basu et al. (1999), we have considered only the longitudinal averages, which contain information about the latitudinal variation in these flows. For this purpose, at each latitude we have summed the spectra obtained for different longitudes in order to get an average spectrum, which has information on the average flow velocity at each latitude. We have studied both the rotational and meridional components of flow velocities.

The rest of the paper is organized as follows: the basic technique used to calculate the horizontal flow velocities using ring diagrams is described in § 2; the results are discussed in § 3, while the conclusions from our study are summarized in § 4.

2. THE TECHNIQUE

We adopt the ring diagram technique (Hill 1988; Patrón et al. 1997) to obtain the three-dimensional power spectra of solar oscillations. We have used data from full-disk Dopplergrams obtained by the MDI instrument of the Solar Oscillations Investigation (SOI) on board *SOHO*. We have used the same spectra that were obtained by Basu et al. (1999). These spectra are based on regions covering about $15^\circ \times 15^\circ$ with 128×128 pixels in heliographic longitude and latitude and centered at latitudes ranging from 60° N to 60° S. Each region was tracked for 4096 minutes, and we have taken averages over 12 spectra covering an entire Carrington rotation in longitude. These spectra are spaced by 30° in longitude of the central meridian, which would correspond to a time interval of about 3273 minutes. Thus there is some overlap between different spectra. Similarly, we have taken spectra centered at different latitudes separated by 5°, and hence there would be considerable overlap in regions covered by spectra centered at neighboring latitudes. The data cover the period from about 1996 May 24 to June 21. Thus summing gives us a time-averaged spectrum for the period covered.

To extract the flow velocities and other mode parameters from the three-dimensional power spectra, we fit a model of the form

$$P(k_x, k_y, \nu) = \left\{\exp\left[A_0 + (k-k_0)A_1 + A_2\left(\frac{k_x}{k}\right)^2 + A_3\frac{k_x k_y}{k^2}\right] \times [S^2 + (1+Sx)^2]\right\}(x^2+1)^{-1} + \frac{e^{B_1}}{k^3} + \frac{e^{B_2}}{k^4}, \quad (1)$$

where

$$x = \frac{\nu - ck^p - U_x k_x - U_y k_y}{w_0 + w_1(k-k_0)}, \quad (2)$$

$k^2 = k_x^2 + k_y^2$ (k being the total wavenumber), and the 13 parameters A_0, A_1, A_2, A_3, c, p, U_x, U_y, w_0, w_1, S, B_1, and B_2 are determined by fitting the spectra using a maximum

likelihood approach (Anderson, Duvall, & Jefferies 1990). Here, k_0 is the central value of k in the fitting interval, and exp (A_0) is the mean power in the ring. The coefficient A_1 accounts for the variation in power with k in the fitting interval, while the A_2 and A_3 terms account for the variation of power along the ring. The term ck^p is the mean frequency, while $U_x k_x$ and $U_y k_y$ represent the shift in frequency due to large-scale flows and the fitted values of U_x and U_y give the average flow velocity over the region covered by the power spectrum and the depth range where the corresponding mode is trapped. The mean half-width is given by w_0, while w_1 takes care of the variation in half-width with k in the fitting interval. The terms involving B_1 and B_2 define the background power, which is assumed to be of the same form as in Patrón et al. (1997). S is a parameter that controls the asymmetry, and the form of asymmetry is the same as that prescribed by Nigam & Kosovichev (1998). This parameter is positive for positive asymmetry (i.e., more power on the higher frequency side of the peak) and negative for negative asymmetry. By setting $S = 0$ we can fit symmetrical Lorentzian profiles.

The fits are obtained by maximizing the likelihood function L or minimizing the function F given by

$$F = -\ln L = \sum_i \left(\ln M_i + \frac{O_i}{M_i} \right), \tag{3}$$

where the summation is taken over each pixel in the fitting interval. The term M_i is the result of evaluating the model given by equation (1) at ith pixel defined by k_x, k_y, and ν in the three-dimensional power spectrum, and O_i is the observed power at the same pixel. To evaluate the quality of the fit we use the merit function (cf. Anderson et al. 1990)

$$F_m = \sum_i \left(\frac{O_i - M_i}{M_i} \right)^2, \tag{4}$$

where the summation is over all pixels in the fitting interval. Ideally, the merit function per degree of freedom should be close to unity. The number of degrees of freedom can be defined as the difference between the number of pixels in the fitting interval and the number of free parameters in the model.

We fit each ring separately by using the portion of the power spectrum extending halfway to the adjoining rings. For each fit, a region extending about ± 100 μHz from the chosen central frequency is used. We choose the central frequency for fit in the range of 2–5 mHz. Power outside this range is not significant. The rings corresponding to $0 \le n \le 6$ have been fitted. In this work we express k in units of $R_\odot^{-1}$, which enables us to identify it with the degree l of the spherical harmonic of the corresponding global mode.

The fitted U_x and U_y for each mode represent an average of the velocities in the x and y directions over the entire region in horizontal extent and over the vertical region where the mode is trapped. We can invert the fitted U_x (or U_y) for a set of modes to infer the variation in horizontal flow velocity u_x (or u_y) with depth. We use the regularized least squares (RLS) as well as the optimally localized average (OLA) techniques for inversion as outlined by Basu et al. (1999). The results obtained by these two independent inversion techniques are compared in order to test the reliability of inversion results. For the purpose of inversion, the fitted values of U_x and U_y are interpolated to the nearest integral value of k (in units of $R_\odot^{-1}$), and then the kernels computed from a full solar model with corresponding value of degree l are used for inversion. Since the fitted modes are trapped in the outer region of the Sun, inversions are carried out for $r > 0.97\, R_\odot$ only.

3. RESULTS

Following the procedure outlined in § 2, we fit the form given by equation (1) to suitable regions of the three-dimensional spectra. We use approximately 900 modes covering $200 \le l \le 1100$ and $2000 \le \nu \le 5000$ μHz for each spectrum. Figure 1 shows some of the fitted quantities for the averaged spectrum obtained from the region centered at the equator. This figure can be compared with Figure 2 in Basu et al. (1999). The asymmetry parameter S is found to be significant and has a negative value for all the modes. The magnitude of S appears to increase with frequency. However, the use of asymmetrical profiles does not appear to affect the fitted half-width or the horizontal velocities U_x and U_y significantly. As with symmetrical profiles, the fitted half-width w_0 appears to increase at low frequencies. This increase is probably artificial since the actual width is less than the resolution limit of the spectra. We have verified that keeping the width fixed during the fit for these modes does not affect the values of U_x and U_y obtained from the fits.

In order to test whether the fit with additional parameter S is indeed better, we show in Figure 2 the merit function (cf. eq. [4]) per degree of freedom for fits to both symmetrical and asymmetrical profiles. It is clear that the merit function has reduced significantly when the additional parameter S is fitted. The value is close to unity for all modes at low n, which can be identified by the ridges in the low-frequency end of Figure 2. The improvement in the fit is not very clear for higher order modes, as the merit function does not appear to reduce significantly. Similar results were found for fits to two-dimensional spectra obtained by averaging over the azimuthal direction (Antia & Basu 1999). In the two-dimensional spectra, too, the f-modes were found to be distinctly asymmetrical (Antia & Basu 1999), while the difference between fits to symmetrical and asymmetrical profiles was progressively less clear for higher order modes, even though the asymmetry parameter S had similar magnitude. This is mainly because the estimated errors increase with n as the corresponding rings in the three-dimensional power spectra get smaller. It may be noted that for symmetrical profiles we have done a number of experiments by including more terms denoting variations in parameters not included in equation (1), but these do not improve the fits significantly and merit function does not reduce perceptibly (Basu et al. 1999). Thus, it appears that some asymmetry is indeed required to get good fits. This asymmetry can be seen clearly in azimuthally averaged spectra shown by Antia & Basu (1999). The asymmetry parameter S shown in Figure 1 is similar to what was found for the two-dimensional fits in Antia & Basu (1999). Hence, it is clear that although it is difficult to visualize asymmetry in three-dimensional fits, the peak profiles are indeed asymmetrical.

There does not appear to be significant difference between the U_x or U_y obtained by fitting symmetrical or asymmetrical profiles to spectra obtained for the equatorial regions. However, at high latitudes the situation becomes somewhat different, as can be seen from Figures 3 and 4, which compare the fits to spectra from regions centered at a

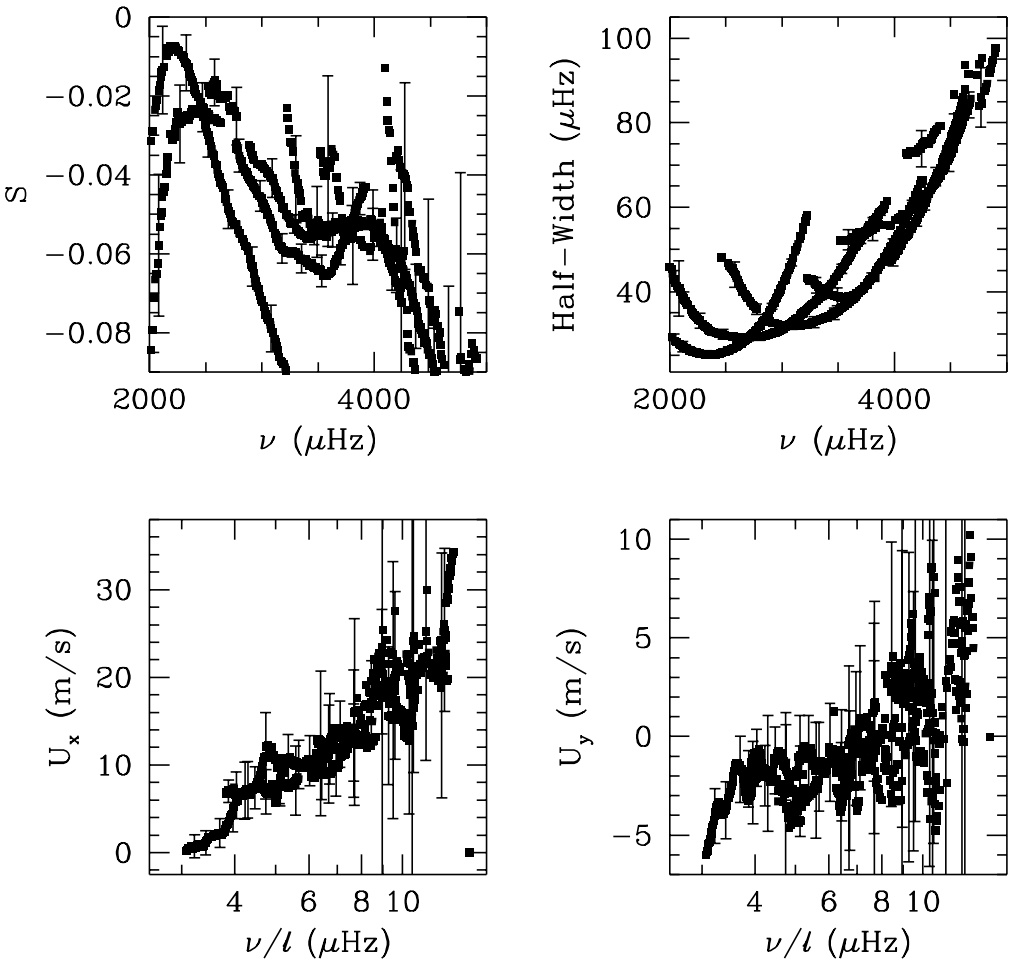

FIG. 1.—Fitted parameters for the summed spectra centered at the equator. This figure shows the asymmetry parameter S, the half-width (w_0), and the average horizontal velocities U_x and U_y. For clarity, only a few error bars are shown.

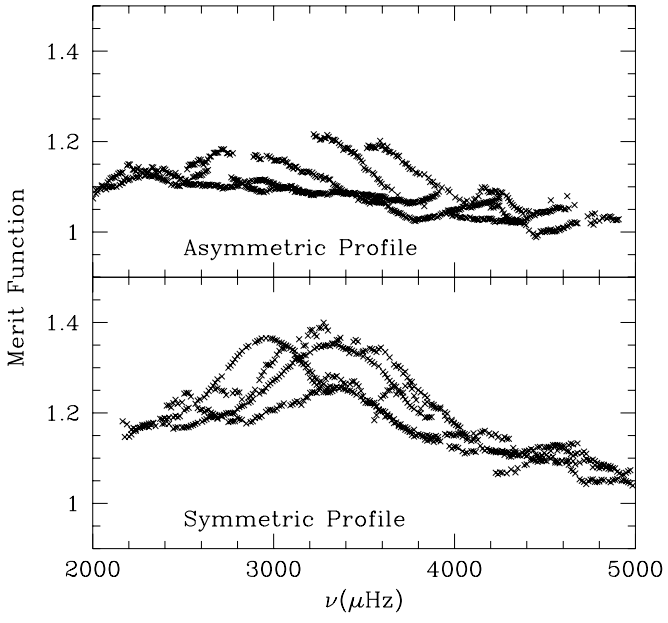

FIG. 2.—Merit function per degree of freedom for fits to the summed spectra centered at the equator using symmetrical and asymmetrical profiles.

latitude of 50° N. It may be noted that even for these latitudes the fitted values for the asymmetry parameter S are similar to what is found for equatorial spectra. However, the fitted values of U_x and U_y are found to be more sensitive to asymmetry at higher latitudes, probably because of effects of foreshortening. The fits with the asymmetrical profile give better results in general, as can be seen from the fact that the ridges in U_x, U_y for different values of n tend to merge better. The difference is particularly significant in U_y. The steep trend in the different ridges corresponding to low n in U_y obtained by fitting symmetrical profiles results in a large number of outliers during the inversions. As a result, we have to weed out a large number of modes to get reasonable inversion results. We weed out all modes that have residuals larger than 4 σ for either U_x or U_y in an RLS inversion with low smoothing. This does not happen when asymmetrical profiles are used. However, the fits are still not perfect at these latitudes even with the use of asymmetrical profiles, and the merit function per degree of freedom is also somewhat larger than unity for low-order modes. Clearly, more terms or a different form is required to improve the fits at high latitudes.

To study the effect of asymmetry on inverted profiles for horizontal velocity components u_x and u_y, we perform

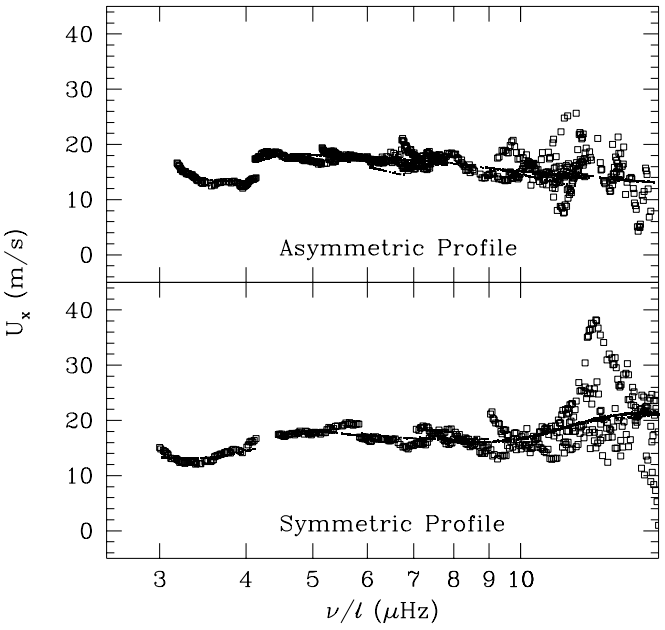

FIG. 3.—Fitted horizontal velocity U_x for fits to the spectra centered at a latitude of 50° N using symmetrical and asymmetrical profiles. The open squares show the fitted U_x, while the small, filled squares, which are merged into a band, show the calculated U_x obtained from the (RLS) inverted velocity profiles shown in Fig. 5.

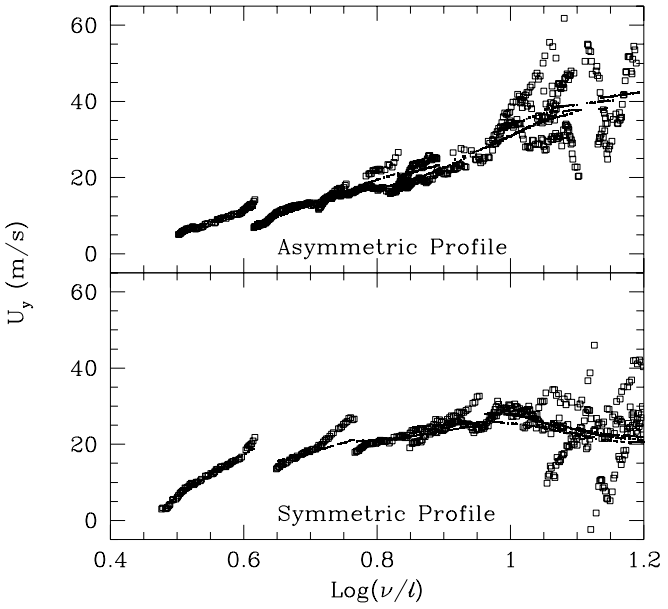

FIG. 4.—Fitted horizontal velocity U_y for fits to the spectra centered at a latitude of 50° N using symmetrical and asymmetrical profiles. The open squares show the fitted U_y, while the small, filled squares, which are merged into a band, show the calculated U_y obtained from the (RLS) inverted velocity profiles shown in Fig. 6.

inversions using both the fits, and the results are shown in Figures 5 and 6. It can be seen that except in deeper layers ($r \lesssim 0.98\ R_\odot$), the inverted results are similar regardless of whether we fit a symmetrical or an asymmetrical profile to the spectra. From the inversion results it is not possible to decide which fit is better, but looking at the residuals and the fitted U_x, U_y in Figures 3 and 4, it appears that asymmetrical profiles would give more reliable results.

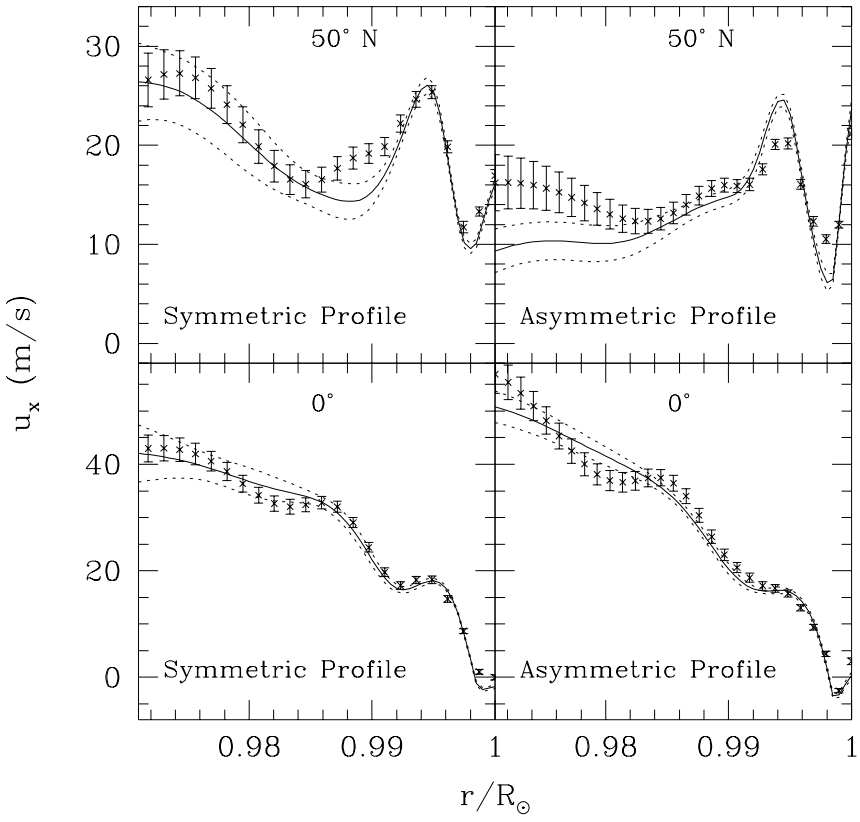

FIG. 5.—Inverted horizontal velocity u_x from fits to the spectra centered at latitudes of 0° and 50° N using symmetrical and asymmetrical profiles. The solid lines show the results obtained using RLS, with dotted lines representing the error limits, while the points with error bars show the results of using the OLA technique.

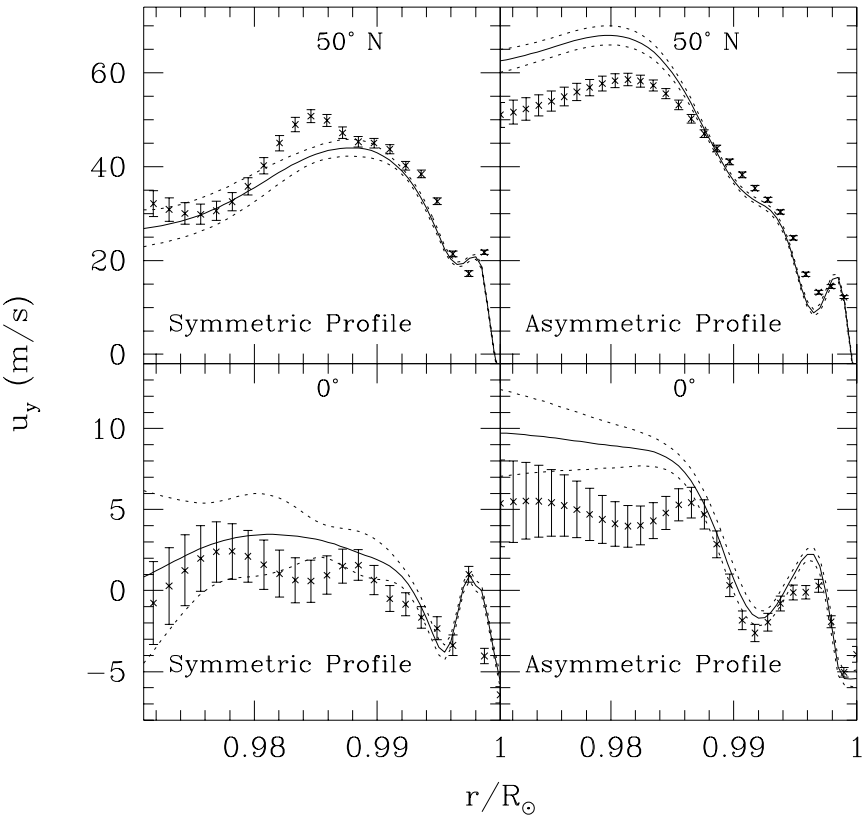

FIG. 6.—Inverted horizontal velocity u_y from fits to the spectra centered at latitudes of 0° and 50° N using symmetrical and asymmetrical profiles. The solid lines show the results obtained using RLS, with dotted lines representing the error limits, while the points with error bars show the results of using the OLA technique.

The rotation velocity at each latitude can be decomposed into the symmetrical part $[(u_N + u_S)/2]$ and an antisymmetric part $[(u_N - u_S)/2]$. The symmetrical part can be compared with the rotation velocity as inferred from the splittings of global modes (Schou et al. 1998) that sample just the symmetrical part of the flow. Since this component is not significantly affected by the asymmetry in peak profiles, we do not show the detailed results. However, the north-south antisymmetric component of rotation velocity is small and its significance is not well established from earlier studies, and hence we reexamine these results with fits to asymmetrical peak profiles. The results for near-surface layers are shown in Figure 7, which can be compared with Figure 7 of Basu et al. (1999). It can be seen that the results are not significantly different from our earlier results. In deeper layers the uncertainties are larger and it is difficult to say anything about this component.

Since there is a distinct improvement in fits to U_y at high latitudes when asymmetrical peak profiles are used, we try to find their effect on meridional flow inferred from ring diagram analysis. Following Hathaway et al. (1996) we try to write the meridional component as

$$u_y(r, \phi) = -\sum_i a_i(r) P_i^1[\cos(\phi)] , \quad (5)$$

where ϕ is the colatitude and $P_i^1(x)$ are associated Legendre polynomials. The first six terms in this expansion are found to be significant, and their amplitudes are shown in Figure 8, which can be compared with Figure 12 of Basu et al. (1999). It can be seen that use of asymmetrical profiles introduces small changes in amplitudes mainly in deeper layers. The amplitudes of all even components increases slightly in deeper layers when asymmetrical profiles are used for fitting. In particular, the $P_4^1(\phi)$ component suggested by Durney (1993) is found to have an amplitude of about 3–4

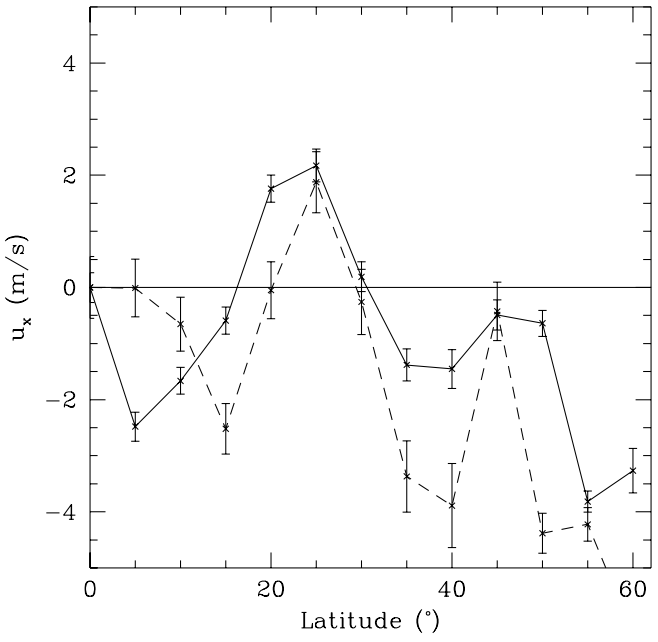

FIG. 7.—Antisymmetric component $[(u_N - u_S)/2]$ of the rotation velocity, plotted as a function of latitude for $r = 0.997\ R_\odot$ (*solid line*) and $r = 0.990\ R_\odot$ (*dashed line*). These results were obtained using the OLA technique.

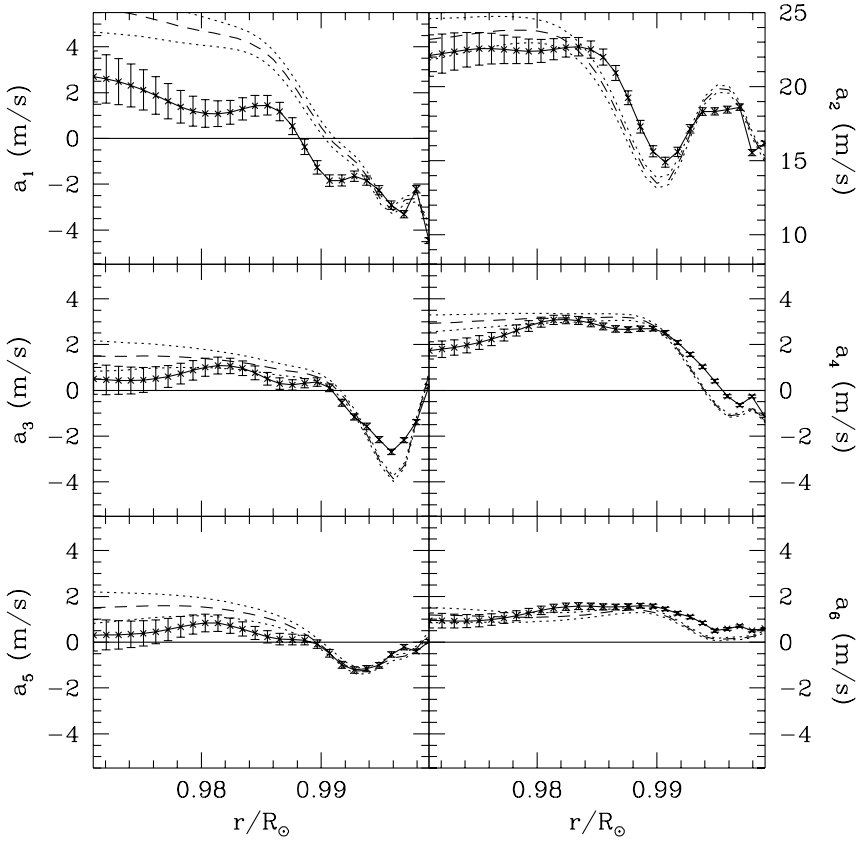

FIG. 8.—Amplitude of various components of meridional velocity as a function of depth, obtained using fits to asymmetrical peak profiles. The solid lines with error bars show the results obtained using OLA inversions, while the dashed line shows the results obtained using the RLS technique, with dotted lines showing the 1σ error limits.

m s^{-1} for $0.97\ R_\odot < r < 0.99\ R_\odot$. There is no indication of any sign change in the meridional flow up to the depth of $0.03\ R_\odot$, which is consistent with results of Braun & Fan (1998). However, the magnitude of the meridional flow velocity that we find (30 m s^{-1}) is much larger than that obtained by Braun & Fan, who find a mean meridional velocity of 10–15 m s^{-1} averaged over latitudes 20°–60°. Clearly, more work is required in order to understand these differences.

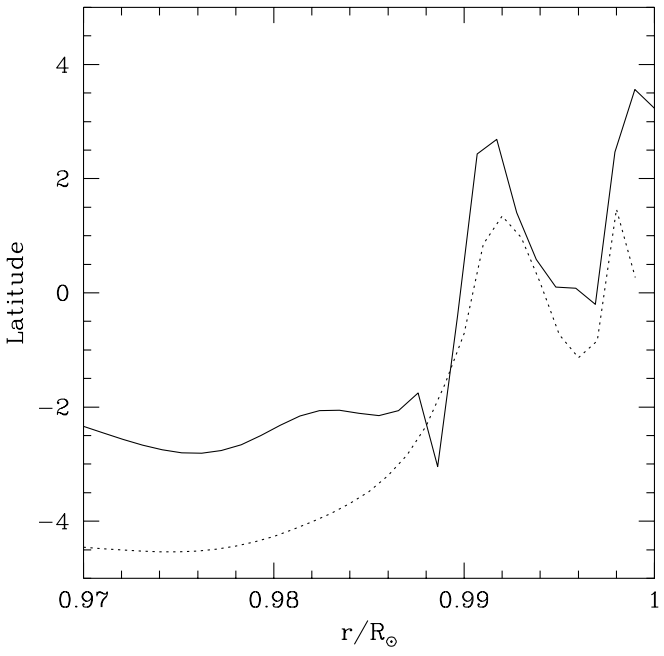

FIG. 9.—Latitude at which $u_y = 0$ is plotted as a function of depth for results obtained using OLA (*solid line*) and RLS (*dashed line*).

We can also find the latitude at which $u_y = 0$, which is the latitude near the equator where the meridional flow diverges toward the two poles. The results shown in Figure 9 can be compared with those obtained by González Hernández et al. (1999). In general we find this point to be much closer to the equator as compared with what they have found. The difference may be due mostly to the fact that we have averaged over all longitudes in one Carrington rotation, and as a result, our error estimates are much lower. For all depths we find that this point is within 4° of the equator and we do not find any chaotic behavior near the surface. Of course, the resolution of inversions is limited to a depth below $r = 0.999\ R_\odot$, since we have used only modes with $l < 1100$, which have lower turning points below this depth. Thus the thin layer near the surface is not resolved by inversions and we cannot expect reliable results there. It is not clear whether the small departure of this point from the equator is significant, since the difference in latitude estimated from the two inversion techniques is comparable to the value. A part of the effect may also be due to systematic errors arising from misalignment in the MDI instrument (Giles et al. 1997), and hence no particular significance may be ascribed to the location of this point.

4. CONCLUSIONS

Using the ring diagram technique applied to MDI data, we have determined horizontal velocities in the outer part

of the solar convection zone ($r > 0.97\ R_\odot$). We find that the use of asymmetrical peak profiles improves the fits to the three-dimensional spectra—as measured by the merit function—significantly. The asymmetry parameter is found to be negative for all the modes; i.e., there is more power on the lower frequency side of the peak. This is the same as what has been found earlier at the low-degree end of the power spectrum (Duvall et al. 1993; Toutain et al. 1998). However, the use of asymmetrical profiles does not affect the fitted velocities substantially.

The inferred meridional flow is dominated by the sin (2θ) component, which has an amplitude of about 30 m s^{-1} in most of the region covered in this study. The $P_4^1(\phi)$ component suggested by Durney (1993) also has a significant amplitude of about 3–4 m s^{-1} in deeper layers. The north-south symmetrical component of the meridional flow is generally small, and the meridional velocity (as a function of latitude) changes sign at a point very close to the equator at all depths. This point marks the region where flow diverges toward the two poles on two sides. The small departure of this point from the equator may not be significant. There is no change in sign of meridional velocity with depth up to about 21 Mm.

This work utilizes data from the SOI/MDI on the *SOHO*. *SOHO* is a project of international cooperation between ESA and NASA. The authors would like to thank the SOI Science Support Center and the SOI Ring Diagrams Team for assistance in data processing. The data-processing modules used were developed by Luiz A. Discher de Sa and Rick Bogart, with contributions from Irene González Hernández and Peter Giles.

REFERENCES

Anderson, E. R., Duvall, T. L., Jr., & Jefferies, S. M. 1990, ApJ, 364, 699
Antia, H. M., & Basu, S. 1999, ApJ, 519, 400
Basu, S., Antia, H. M., & Tripathy, S. C. 1999, ApJ, 512, 458
Braun, D. C., & Fan, Y. 1998, ApJ, 508, L105
Durney, B. R. 1993, ApJ, 407, 367
Duvall, T. L., Jr., Jefferies, S. M., Harvey, J. W., Osaki, Y., & Pomerantz, M. A. 1993, ApJ, 410, 829
Giles, P. M., Duvall, T. L., Jr., Scherrer, P. H., & Bogart, R. S. 1997, Nature, 390, 52
González Hernández, I., Patrón, J., Bogart, R. S., & The SOI Ring Diagram Team. 1999, ApJ, 510, L153
Hathaway, D. H., et al. 1996, Science, 272, 1306
Hill, F. 1988, ApJ, 333, 996
Nigam, R., & Kosovichev, A. G. 1998, ApJ, 505, L51
Patrón, J., et al. 1997, ApJ, 485, 869
Schou, J., et al. 1998, ApJ, 505, 390
Toutain, T. 1993, in Proc. Sixth IRIS Workshop, ed. D. O. Gough & I. W. Roxburgh (Cambridge: Univ. Cambridge Press), 28
Toutain, T., Appourchaux, T., Fröhlich, C., Kosovichev, A. G., Nigam, R., & Scherrer, P. H. 1998, ApJ, 506, L147